AIAA JOURNAL
Vol. 33, No. 5, May 1995

Skin-Friction Measurements in Three-Dimensional, Supersonic Shock-Wave/Boundary-Layer Interaction

Jeffrey K. Wideman*
University of Missouri, Columbia, Missouri 65201
James L. Brown†
NASA Ames Research Center, Moffett Field, California 94035
John B. Miles‡
University of Missouri, Columbia, Missouri 65201
and
Oktay Özcan§
Istanbul Technical University, 80626 Istanbul, Turkey

The experimental documentation of a three-dimensional shock-wave/boundary-layer interaction in a nominal Mach 3 flow is presented. The model consisted of a sting-supported cylinder, aligned with the freestream flow, and a 20-deg half-angle conical flare offset 1.27 cm from the cylinder centerline. Surface oil flow, laser light sheet illumination, and spark schlieren photography were used to document the flow topology. Extensive surface-pressure and skin-friction measurements were made throughout the interaction region. A laser interferometric skin-friction instrument was employed to acquire the skin-friction data. Resolved skin-friction measurements of C_{fx} and C_{fz} were made within the highly swept three-dimensional separated regions. The skin-friction data will be of particular value for turbulence modeling and computational fluid dynamics validation.

Nomenclature

C_f = local skin-friction coefficient, $\equiv 2\tau/\rho_\infty U_\infty^2$
$C_{1,2,3}$ = constants
h = local oil thickness
k_i = incremental fringe number
M_∞ = freestream Mach number
N = fringe number
N_o = reference fringe number
n_o = refractive index of oil
P = local surface pressure
P_t = total pressure
P_∞ = freestream static pressure
Re = Reynolds number
r = radial coordinate from cylinder centerline
T_t = total temperature
T_∞ = freestream static temperature
t = oil-flow time
t_i = incremental oil-flow time
t_o = reference oil-flow time
U_∞ = freestream velocity
x = streamwise coordinate, also distance from oil leading edge to measurement beam
x_a = attachment location
x_s = separation location
z = transverse coordinate
β = surface flow angle
δ = boundary-layer thickness
θ_t = refracted beam angle
λ = wavelength of light
ν_o = kinematic viscosity of oil
ρ_o = density of oil
ρ_∞ = freestream density
τ = local wall shear stress
ϕ = azimuthal coordinate

Received Nov. 23, 1993; presented as Paper 94-0314 at the AIAA 32nd Aerospace Sciences Meeting, Reno, NV, Jan. 10–13, 1994; revision received July 26, 1994; accepted for publication Aug. 9, 1994.

*Ph.D. Student. Student Member AIAA.
†Research Scientist, Modeling and Experimental Validation Branch.
‡Professor of Mechanical and Aerospace Engineering. Member AIAA.
§Professor, Department of Aeronautics and Astronautics, Maslak.

Introduction

THE flowfield surrounding aerodynamic vehicles can be quite complex. Practical flows are typically compressible, turbulent, and three dimensional. In addition, at supersonic speeds shock waves exist which interact with flight surface boundary layers. The adverse pressure gradient associated with shock-wave/boundary-layer interactions (SW/BLI) can cause the boundary layer to separate, thus altering aircraft performance. Hence, there is a need to better understand and predict these SW/BLI.

Over the years, computational fluid dynamics (CFD) has augmented experimental research on SW/BLI. Although the idea of full computational simulation of flowfields in place of wind-tunnel documentation is appealing, much work is required before complete computational solutions to turbulent three-dimensional SW/BLI problems can be reliably achieved. In solving the Navier–Stokes equations, closure of the equation set is achieved by modeling the turbulence. These turbulence models need to be developed with reliance on measurements of the physical phenomenon of the interaction. There is also a need to provide experimental data to validate the computational results from CFD. Thus, experiments and computations are complementary tools that can extend the present understanding of fluid dynamics and produce methods by which SW/BLI can be accurately predicted.

The present building-block experiment (see also Ref. 1) was undertaken, in the context of previous related axisymmetric and unsteady three-dimensional SW/BLI studies,[2–5] with the goal of acquiring accurate data in a steady three-dimensional SW/BLI to guide turbulence modeling development and for CFD code validation. Because of the scarcity of accurate skin-friction data in SW/BLI, the emphasis of this study was on the acquisition of skin-friction data. A laser interferometric skin-friction (LISF) instrument was used to acquire the skin-friction data in this complex flow characterized by large pressure and shear-stress gradients. The dataset for this experiment is available on the disk included in Ref. 1 or via e-mail from the second author.

Table 1 Tunnel operating conditions

P_t, kPa (1.7 atm)	172.37
T_t, K	280
P_∞, kPa	5.54
T_∞, K	105
ρ_∞, kg/m^3	0.184
M_∞	2.89
U_∞, m/s	593
Re, m^{-1}	15.0×10^6
δ, cm	1.10

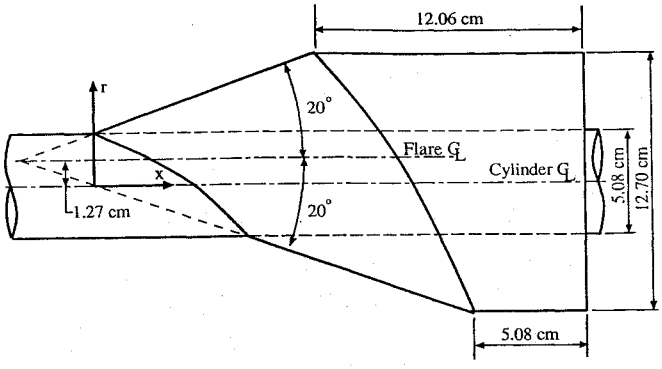

Fig. 1 Schematic of 20 deg/1.27 cm offset three-dimensional flare.

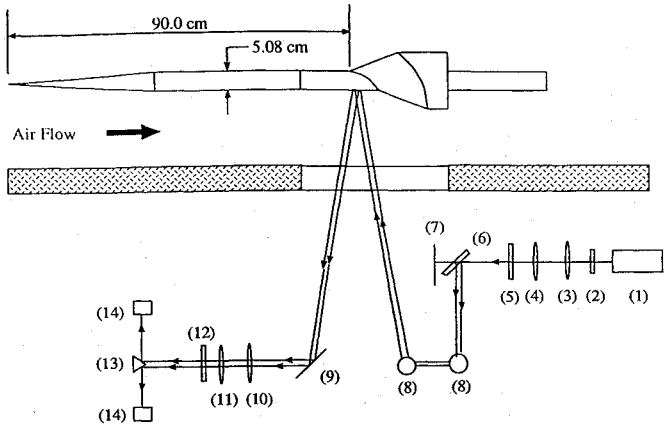

Fig. 2 Schematic of LISF instrument; 1) 5 mW helium-neon laser, 2) spatial filter, 3) focusing lens, 4) focusing lens, 5) neutral density filter, 6) interferometric flat, 7) beam stop, 8) vertical assembly of mirror, 9) mirrors, 10) collimating lens, 11) focusing lens, 12) 0.6328 micron filter, 13) reflective prism, and 14) photodiodes.

Experimental Description

Flow Model and Test Conditions

The experimental study was conducted in the NASA Ames Research Center High Reynolds Channel I facility. A Mach 3 nozzle was employed for the study. The test section was 25.4 cm wide by 38.1 cm high. An axisymmetric turbulent boundary layer developed on a 5.08-cm-diam cylinder aligned with the tunnel axis (Figs. 1 and 2). An instrumented three-dimensional flare slid over and was secured to the cylinder. The flare was fabricated as a 20-deg half-angle axisymmetric cone but with its centerline displaced 1.27 cm from the cylinder centerline. The flare was terminated with a 12.70-cm-diam afterbody, the centerline of which matched that of the cylinder. The two azimuths of symmetry were along $\phi = 0$ and $\phi = 180$ deg. The x-ϕ-r cylindrical coordinate system was aligned with the cylinder centerline with $x = 0$ located at the leading edge of the offset flare. The model was chosen because the resulting shock system was found to be steady by comparison of numerous spark schlieren photographs. Table 1 presents the tunnel operating conditions.

Pressure Measurement

The pressure acquisition system was similar to that of Olsen and Seegmiller[6] but with adaptations to enhance accuracy for supersonic work. Surface pressures were measured through pressure taps on the cylinder and on the three-dimensional flare by an electronic scanning pressure system. The differential pressure transducers were referenced to the upstream static pressure, which was sensed by a 1000 Torr absolute Barocel. Each transducer was calibrated prior to every run. The total pressure was sensed by a 100-psi differential Barocel referenced to atmosphere. The cylinder possessed four rows of pressure taps along azimuths spaced 90 deg apart. The flare contained 13 rows of 22 pressure taps every 15 deg so as to document one region of symmetry ($\phi = 0$–180 deg).

Skin-Friction Measurement

Theory

Tanner and Blows[7] introduced the LISF technique. In addition to subsequent work done by Tanner and his associates, other significant studies involving the LISF technique have been performed at NASA Ames Research Center,[8,9] Pennsylvania State University,[10] and California Institute of Technology.[11] The LISF technique is nonintrusive and quasidirect in determining the wall shear stress. Since its inception, the LISF technique has been applied to increasingly complex flows. It is in complex flows, such as SW/BLI, that the advantages of the LISF technique are realized because it is capable of performing accurate skin-friction measurements in flows characterized by large pressure and shear-stress gradients. Reference 1 includes a review of the LISF technique and further information pertaining to this study.

The LISF technique requires a thin oil film on the test surface. The oil film thickness decreases with time due to the wall shear stress of the air flow. To measure the time-dependent thickness of this oil film, a laser beam is directed toward the oil. A portion of the laser beam is reflected from the air-oil interface and another portion is reflected from the oil-model interface. The light reflected from these two interfaces is imaged onto a photocell using collecting lenses. The path length of the light reflected from these two interfaces from the laser to the photocell differs according to the oil film thickness. As the oil film thins, a time sequence of interference fringes occurs at the photocell due to this varying path length difference. The time-varying voltage output of the photocell is referred to as the fringe record and consists of a series of peaks and valleys related to the time-varying oil thickness.

An oil film subjected to a constant shear stress will assume a wedge shape. The basic hydrodynamic LISF equation[7] for this case is

$$\tau = \rho_o \nu_o x / ht \tag{1}$$

From refraction theory, the oil film thickness can be determined from the equation

$$h = N\lambda / 2n_o \cos\theta_t \tag{2}$$

Combining Eqs. (1) and (2), the expression for the wall shear stress becomes

$$\tau = 2n_o \rho_o \nu_o x \cos\theta_t / N\lambda t \tag{3}$$

Under three-dimensional flow conditions, the skin-friction component in a particular direction is measured by applying the oil on the model surface so that the oil leading edge forms a line that is normal to the desired measurement direction.

Apparatus

A schematic of the LISF instrument is shown in Fig. 2. The transmitting side of the instrument included a 5.0-mW, 0.6328-μm wavelength helium-neon laser. A spatial filter and lens assembly expanded the beam and allowed adjustment of the beam focus location. By positioning an interferometric flat at 45 deg to the incident beam, the reflection from the front and back of the flat provided two beams of the same intensity with a 5-mm spacing. A mirror assembly directed the two beams toward the model at a near-normal incidence

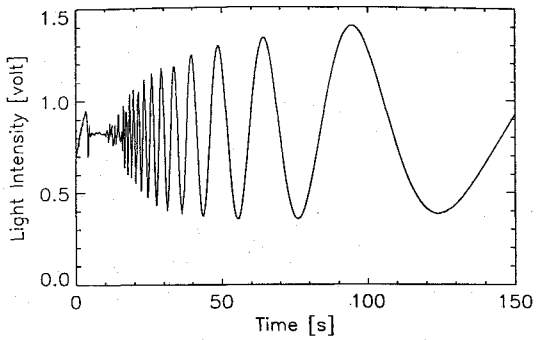

Fig. 3 LISF signal from plastic surface over MonoKote.

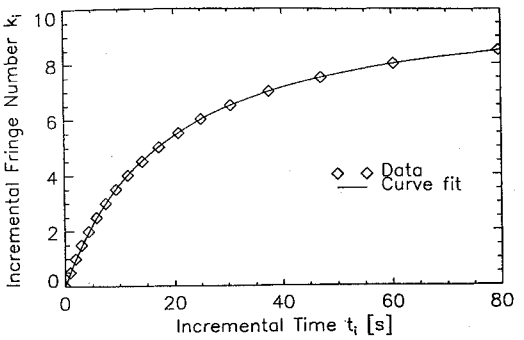

Fig. 4 Curve fit of incremental fringe number vs time.

angle. Even though two beams were available, the single-beam approach was predominately used to perform the LISF measurements because of the relatively small scale of the interaction under study.

The receiving side of the instrument included lenses to focus the reflected light from the two measurement spots onto different sides of a reflective-coated prism. The prism directed the beams into two separate photodiodes. The signals were amplified, low-pass filtered, and digitized. The laser and optics were mounted on an optical table positioned by stepper motors. Dow Corning 200 silicone oils were used with three different viscosities: 200, 500, and 1000 cs.

The properties of the model surface on which LISF measurements are performed are important. The surface should be smooth and free of imperfections and scratches. Furthermore, the intensity of the beam reflected from the oil-model interface should be comparable to the intensity of the beam reflected from the air-oil interface to maximize signal visibility. An alternative to polishing the test surface was sought. First, a layer of MonoKote was applied to the surface. Then a clear plastic[12] with adhesive backing was placed over the MonoKote. The clear plastic provided a smooth surface and also the intensity of the oil-plastic interface reflection was comparable to the intensity of the air-oil interface reflection. The resulting signal visibility was typically 60% (Fig. 3). The ordinate zero level in the plot is the actual zero voltage level. The MonoKote covered the model surface and absorbed the unreflected portion of the incident beam. The MonoKote also minimized interference from the pressure taps on the LISF measurements.

Since the oil viscosity was temperature sensitive, an accurate measure of surface temperature was crucial for the LISF technique. The oil was typically only several laser wavelengths thick so the oil was assumed to be at the surface temperature. The flare was fabricated with an internal-lead surface thermocouple located at $x = 12.5$ cm along $\phi = 90$ deg. Extensive effort was put forth to verify the accuracy of this thermocouple. One consideration was the possible effect of the plastic between the model and the oil. The effect, however, was negligible because the temperature difference across the plastic was estimated to be only 0.6 K. To confirm the reading of the single internal-lead thermocouple, additional commercial thermocouples were temporarily mounted on the model surface at several locations. These temporary thermocouples confirmed the internal-lead thermocouple was accurate to within 4 K. These temporary thermocouples were then removed to avoid flow interference. With only the one internal thermocouple then available, the temperature of the entire model was assumed to equal the reading from this thermocouple. In light of this assumption and the inherent difficulty in measuring the surface temperature, the oil viscosity term was the largest source of uncertainty in the skin-friction results.

Data Reduction

The pertinent quantity to be determined from the LISF fringe record is the product of the fringe number and oil-flow time (Nt). The following analysis was suggested by Bouslog[13] to accurately determine a value for the fringe-time product from LISF data. Equation (3) can be rearranged to obtain

$$\frac{1}{N} = \frac{\tau\lambda}{2n_o\rho_o v_o x\cos\theta_t}\, t = C_1 t \tag{4}$$

where C_1 may be assumed constant due to the steady shear stress and oil temperature as given by

$$C_1 \equiv \frac{\tau\lambda}{2n_o\rho_o v_o x\cos\theta_t} \tag{5}$$

A reference fringe extremum (peak or valley) can be arbitrarily selected from the experimentally obtained fringe record. A reference fringe number N_o and oil-flow time t_o can be symbolically assigned to this reference fringe extremum even though the actual physically related values for N_o and t_o are unknown. The motivation is to accomplish an origin shift (of unknown magnitude N_o and t_o) from the unknown physical origin for N and t to a new origin located at the reference fringe since the observed incremental fringe number k_i and the observed incremental oil-flow time t_i of the data are known relative to this reference fringe. This origin shift furthermore accounts for tunnel startup transients, etc. since a virtual origin for the steady-state data becomes implicitly defined. Note that Eq. (4) yields the relationship between N_o and t_o

$$1/N_o = C_1 t_o \tag{6}$$

Proceeding through the rest of the fringe record, each successive extremum may be assigned an incremental fringe number k_i that is incremented by one-half for each extremum. Also determined for each fringe extremum is the time since the reference fringe t_i which is the observed incremental oil-flow time. Naturally, for the reference fringe $k_i = 0$ and $t_i = 0$. Note that for each extremum there exists a simple coordinate transformation between the physically related (N, t) and the observed (k_i, t_i) given by

$$N = N_o - k_i, \qquad t = t_o + t_i \tag{7}$$

Equation (4) in terms of the observed quantities (k_i, t_i) becomes

$$\frac{1}{N_o - k_i} = C_1(t_o + t_i) = C_1 t_o + C_1 t_i \tag{8}$$

Recalling Eq. (6) and defining $C_2 \equiv t_o/N_o$, and $C_3 \equiv 1/N_o$, Eq. 8 becomes

$$k_i = t_i/(C_2 + C_3 t_i) \tag{9}$$

The values for the incremental fringe number and time, k_i and t_i, in Eq. (9) are obtained from the LISF fringe record once a reference fringe is chosen and plotted (Fig. 4). Note the data point for the reference fringe is located at the plot origin. Also, the time at which the flow began need not be known for this analysis. The two unknown constants C_2 and C_3 are determined by performing an iterative least-squares curve fit procedure[1,14] of Eq. (9) to the incremental fringe number vs time data as shown in Fig. 4. The constant C_1 can next be determined from

$$C_1 = C_3^2/C_2 \tag{10}$$

Rearranging Eq. (5), the local wall shear stress can be calculated from

$$\tau = 2n_o\rho_o v_o x\cos\theta_t C_1/\lambda \tag{11}$$

Finally, the shear stress can be nondimensionalized by freestream conditions using

$$C_f \equiv 2\tau/\rho_\infty U_\infty^2 \tag{12}$$

In the preceding derivation, the surface temperature was assumed steady. This assumption was not valid for this supersonic test. The time variation of the surface (and oil) temperature was accounted for by using a corrected time based on the temperature variation.[1] Also, pressure and shear-stress gradients can affect the oil film shape and thus affect the LISF measurements. These effects are minimized due to the oil film being typically only several wavelengths of light thick. Using the analysis of Monson et al.,[8] pressure-gradient and shear-stress-gradient corrections to the measured shear-stress values for each LISF measurement were determined. These corrections were found to be negligible and thus were not incorporated.

Results and Discussion

Surface Flow Visualization

Surface oil-flow visualization revealed many details of the surface topology. The surface oil flows primarily employed oil dots placed by a small brush on the model prior to a tunnel run. The oil mixture consisted of titanium dioxide powder mixed into vacuum pump oil to obtain the desired viscosity. A small amount of oleic acid is first added to the vacuum pump oil to prevent coagulation of the powder. The locations of the nodes and saddles discussed subsequently were measured to within 2 mm and are tabulated in Ref. 1.

Figures 5 and 6 are two views of the model after one run. Figure 7 shows an oil pattern after another run and provides more detail in the region near the $\phi = 180$ deg symmetry line. The flow in these figures

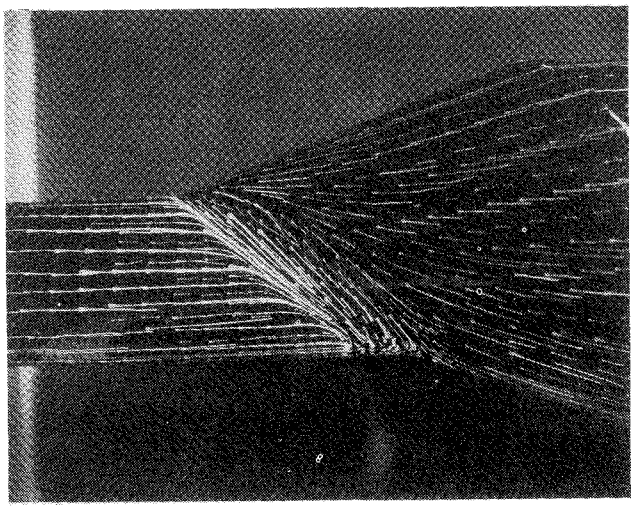

Fig. 5 Oil flow visualization, view from $\phi \approx 45$ deg.

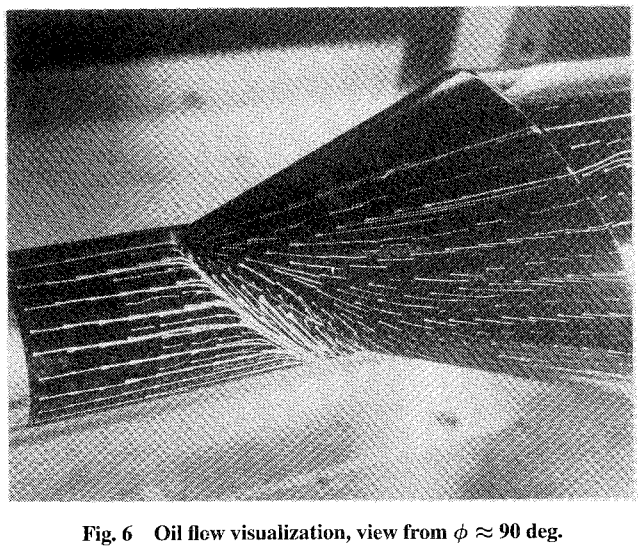

Fig. 6 Oil flow visualization, view from $\phi \approx 90$ deg.

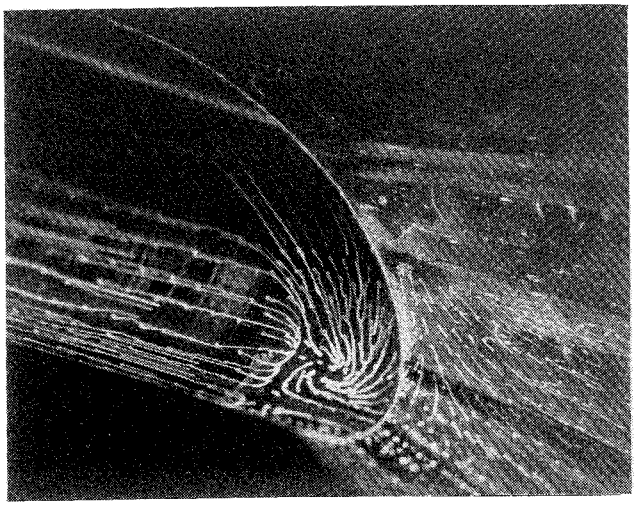

Fig. 7 Oil flow visualization, view from $\phi \approx 165$ deg.

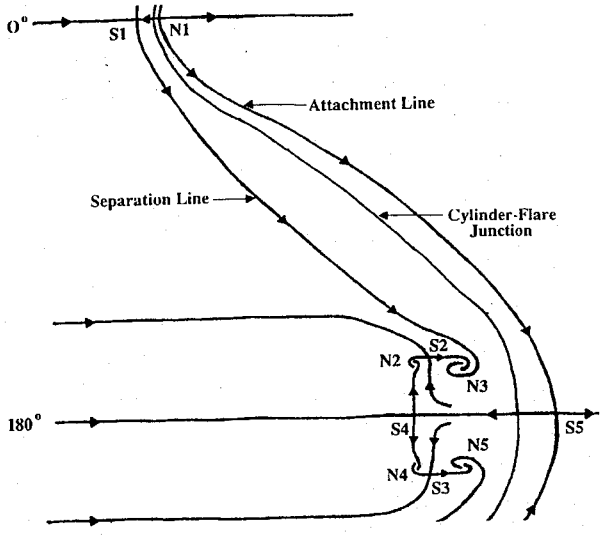

Fig. 8 Unwrapped postulated skin-friction pattern.

was from left to right. The postulated skin-friction pattern is shown in Fig. 8. There were a total of seven nodes and five saddles which satisfied the topological law[15] that for a closed three-dimensional surface, the number of nodes must exceed the number of saddles by two (7 nodes-5 saddles = 2). Although not shown, there was a node of attachment ($N6$) at the upstream tip of the cylinder and a node of separation ($N7$) at the rear of the cylinder.

Referring to Figs. 5–8, a saddle of separation ($S1$) and a node of attachment ($N1$) were formed along $\phi = 0$. The separation lines that emanated from the saddles of separation along $\phi = 0$ ($S1$) and $\phi = 180$ deg ($S4$) terminated into different foci of separation ($N3$ and $N2$). Another saddle of separation ($S2$) was located between these two foci. A saddle of attachment ($S5$) was formed at the intersection of the attachment line and $\phi = 180$ deg and was directly connected to the saddle of separation $S4$. This type of connection had been thought to be unstable. It is possible that the oil flow resolution was not adequate to distinguish other singular points in the vicinity of saddle $S5$. Yet Chapman[16] considered saddle-to-saddle connections possible under conditions of strong symmetry. Other references[17,18] also feature such connections. Thus, the present saddle-to-saddle connection along $\phi = 180$ deg is plausible as a consequence of flow symmetry.

Based on the surface oil flows, schlieren, and laser light sheet visualization techniques, a postulated flow structure was developed. The flow structure along $\phi = 0$ deg consisted of separation, which spiraled into a vortex, followed by attachment on the flare. The vortex continued along the model on both sides of symmetry. Near $\phi = 180$ deg, the postulated flow structure included two main vor-

tices which left the surface at the two largest foci of separation ($N3$ and $N5$) and remained embedded within the boundary layer on the flare.

An important consideration in separated SW/BLI studies is whether the shock system is steady or undergoes rapid oscillations in position and pressure level. Large-scale shock unsteadiness may greatly increase levels of measured Reynolds stresses, thereby complicating turbulence modeling of such flows, see Brown et al.[2] If the shock system is curved as in the present case, a comparison of spark schlieren photographs taken at different times will clearly reveal changes in instantaneous shock position, see the unsteady three-dimensional SW/BLI study of Kussoy et al.[3] For the present study, the shock system was thus verified to be steady.

Surface Pressure

The surface pressure data presented here were acquired with the model rotated so that the desired azimuths were aligned with the top of the cylinder. The accuracy of the pressure measurements is estimated[1,6] based on repeatability and uncertainty analysis to be within 1% of P/P_t. The pressure distributions along individual azimuths are shown in Fig. 9. A contour plot of the pressure data is shown in Fig. 10. The contours reveal the steep streamwise pressure gradient along $\phi = 0$. There is also a steep streamwise pressure gradient in the region between $\phi = 150$ and 180 deg, which occurs on the cylinder in the vicinity of separation. The significant transverse pressure gradient is apparent in the plot between $\phi = 15$ and 150 deg. The direction of the maximum pressure gradient appears to be roughly normal to the cylinder-flare junction. The maximum pressure gradient in the highly swept-flow region from $\phi = 30$ to 105 deg appears to occur in the vicinity of reattachment. The plateau regions visible in the individual distributions are evident in the contour plot downstream of the initial pressure rise and upstream of the cylinder-flare junction from $\phi = 30$ to 180 deg. The wavy contour line in the region near the cylinder-flare junction is due to the disparity of the amount of data taken in the transverse direction as compared to the streamwise direction and is an artifact of the contour calculation. The contour plot is overlaid with the interpretation from the oil-flow visualization results. The scale of Fig. 10 was chosen to allow the overlay of Fig. 8. Note that the singular points identified from the oil-flow visualization do not leave an obvious footprint in the pressure contours.

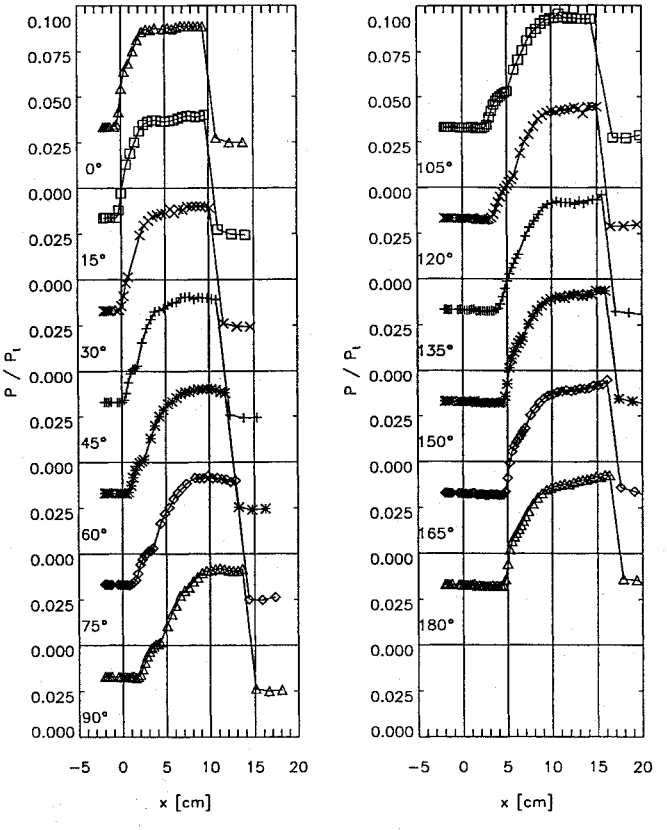

Fig. 9 Surface pressure distributions.

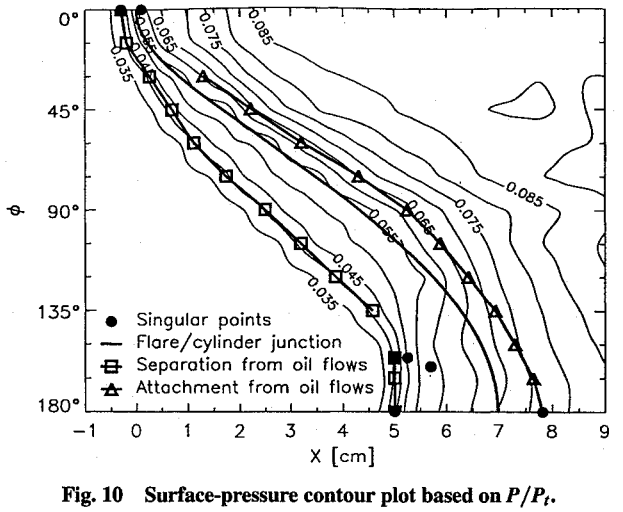

Fig. 10 Surface-pressure contour plot based on P/P_t.

Skin Friction

In contrast to the pressure measurements (for reasons of optical access), the skin-friction data were acquired with the model rotated so that the desired azimuths were aligned with the side of the cylinder. A limited number of supplementary pressure measurements (not shown in Fig. 9 but available in Ref. 1) were obtained for these model rotations so as to verify that the flow with the model aligned with the side of the cylinder was not significantly different than when the model was aligned with the top of the cylinder.

The accuracy of the skin friction measurements based on repeatability and a detailed uncertainty analysis[1] is estimated to be within ±8%. The largest source of uncertainty in the skin friction uncertainty analysis is the oil viscosity term due to the difficulty in determining the surface temperature. Another estimate of skin friction measurement accuracy based on comparison with other measurement techniques is given in the next section but is consistent with this estimate.

Measurements in Undisturbed Boundary Layer

To further assess the accuracy of the LISF measurements, a comparison was made with results from other techniques in the undisturbed boundary layer upstream of the interaction. There are instruments that accurately measure the skin friction in boundary layers free of pressure- and shear-stress-gradient effects. However, such instruments were not available for this study. Thus, other standards for comparison were pursued. One standard employed a similarity technique to deduce the skin friction from experimental mean-velocity profiles. The velocity profiles were acquired with a laser Doppler velocimeter. The analysis of Sun and Childs[19] was applied to the experimental velocity profiles by curve fitting their wall-wake correlation to the data. The mean of the deduced skin-friction results was $C_{fx} = 0.00144(\pm 2\%)$. A second standard was the Van Driest (II) theory[20] which predicted a skin-friction coefficient of $C_{fx} = 0.00156$. The mean skin-friction coefficient from the LISF measurements was $C_{fx} = 0.00149(\pm 5\%)$ which was 3% higher than the deduced value from the velocity profile and 5% lower than the value predicted by the Van Driest (II) theory. Since the LISF result was between the two selected standards, confidence existed that the LISF result in the undisturbed boundary layer was indeed accurate to the ±8% cited earlier.

Measurements Along $\phi = 0$

As the boundary layer initially encountered the streamwise pressure gradient, the mean flow near the wall was retarded decreasing the skin friction (Fig. 11). Extrapolation of the skin-friction data upstream of separation to the zero skin-friction level indicated that

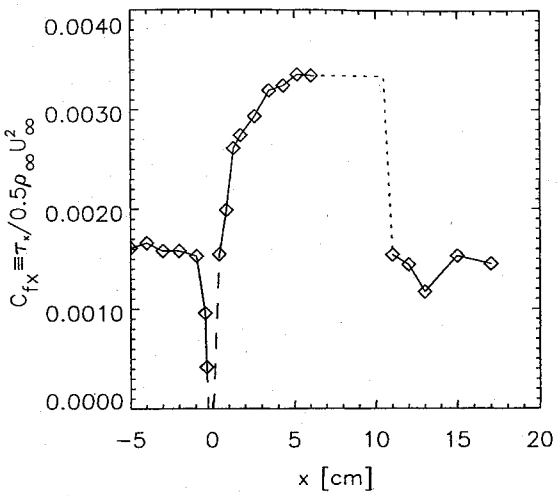

Fig. 11 Streamwise LISF measurements along ϕ = 0.

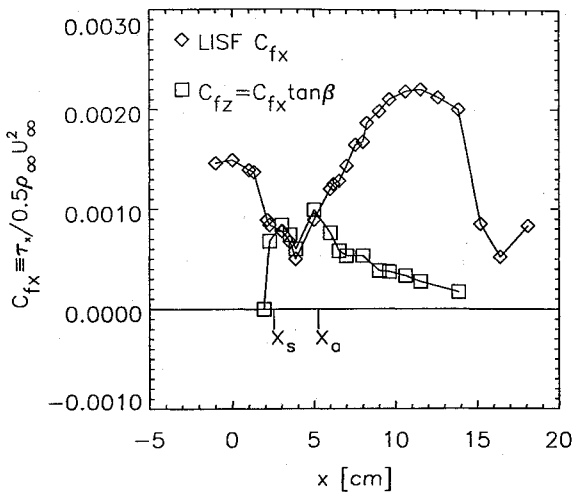

Fig. 12 Streamwise LISF measurements along ϕ = 90 deg.

separation occurred at $x_s = -0.27$ cm. This extrapolated location was comparable to the separation location from the surface oil flow visualization which was estimated to be at $x_s = -0.30$ cm. Continuing along this line of symmetry, it is expected that the skin friction would be negative in the separated region since the oil flow visualizations revealed that the flow direction was opposite to the freestream direction. However, the distance between the separation line and cylinder-flare junction along $\phi = 0$ was too small to perform a measurement. Dashed lines in Fig. 11 indicate the expected distribution just upstream of separation and downstream of attachment.

At the first measurement location downstream of attachment, the skin friction increased from the anticipated negative values in the separated region to a level comparable to the undisturbed value. We argue the basis for this high skin-friction level for the reattaching $\phi = 0$ boundary layer is that the inner portion of the initial boundary layer becomes entrained in the separation vortex where this fluid then flows down either one or the other side. Note that in contrast to a closed two-dimensional separation bubble, three-dimensional separation can entrain fluid. As the flow proceeds over the separated region for $\phi = 0$, the innermost low-momentum fluid of the boundary layer may be entrained into the three-dimensional separation vortex. Thus, the flow that reattached for $\phi = 0$ may consist of only the outer, more energetic fluid of the original boundary layer, which would then impose a steep velocity gradient at the surface, and thereby lead to a high skin-friction level. It is hoped that flowfield measurements to be reported and Navier–Stokes solutions will provide insight into the interesting role flow topology plays in this and other aspects of this complex three-dimensional interaction.

Although the pressure plateau was reached by $x = 2.35$ cm, the skin friction continued to increase past that location and eventually reached a skin-friction plateau near $x = 5.17$ cm. The skin-friction coefficient along $\phi = 0$ increased to a value 2.25 times the undisturbed upstream boundary-layer value (a 125% increase). Thus, one effect of the interaction was a doubling of the local skin friction along this azimuth. The $\phi = 0$ pressure measurements (not shown, see Ref. 1) for this model rotation ($\phi = 0$ of the model aligned with the side of the cylinder) did indicate an extraneous Mach wave that probably originated from the tunnel wall and impinged near the aft end of the flare ramp. As a consequence, the skin-friction measurements in this vicinity also exhibited an anomalous spike and are not shown.

Measurements Along ϕ = 90 deg

The flow along $\phi = 90$ deg was not only affected by the streamwise pressure gradient but also by the transverse pressure gradient. After an initial drop, the streamwise skin friction leveled out just prior to separation and maintained a slightly decreasing trend to a location just inside the three-dimensional separation (Fig. 12). Three-dimensional separation does not imply that the streamwise skin friction should be negative. Note that for the streamwise data along $\phi = 90$ deg, the skin friction remained positive even in the skewed separated region. The oil flow visualizations indicated that the separation line was at $x_s = 2.50$ cm at which point the estimated streamwise skin friction was $C_{fx} = 0.00080$.

Toward the middle of the separated region along $\phi = 90$ deg, the skin-friction distribution reached a minimum at $x = 3.85$ cm. Between $x = 3.75$ and 4.00 cm, the pressure was nearly constant, increasing by only 0.4%. The one measurement within the separated region on the flare indicated a sharp increase in skin friction. The streamwise skin friction was higher in the vicinity of attachment than it was near separation. Attachment was located on the flare at $x_a = 5.25$ cm as indicated by oil flow visualizations. The streamwise skin friction began to level off near $x = 10.0$ cm, which was slightly downstream from the plateau in the pressure distribution. The peak value for the streamwise skin-friction coefficient along $\phi = 90$ deg was $C_{fx} = 0.00220$ and was an increase of 48% over the undisturbed level.

The values for the transverse component of skin friction (Fig. 12) were resolved from the streamwise LISF measurements and the flow-angle data from oil flow visualization. As a result of the transverse pressure gradient, the flow in the upstream influence region along $\phi = 90$ deg turns away from the freestream direction. The transverse skin-friction coefficient increased from zero in the undisturbed boundary layer to a value of $C_{fz} = 0.00068$ at $x = 2.25$ cm. The transverse skin-friction coefficient reached a relative maximum at $x = 3.00$ cm, 0.50 cm downstream of separation. The transverse skin friction reached another maximum just upstream of attachment. Downstream of attachment, the transverse skin-friction decreases asymptotically toward zero as the flow up the ramp turns back toward the streamwise direction. Direct LISF measurements of the transverse skin friction were also performed at six locations upstream and within the separated region. These direct measurements of the transverse skin friction agreed with the resolved values to within 5%. The maximum flow-turning angle with respect to the freestream direction was determined from the oil flow visualization to be 50 deg at $x = 3.85$ cm.

Measurements Along ϕ = 180 deg

The initial effect of the interaction along $\phi = 180$ deg was a decrease in the streamwise skin friction just upstream of $x = 4.5$ cm. Within the separated region, the flow direction along $\phi = 180$ deg was opposite to the freestream direction. Skin-friction measurements were performed at five locations within the separated region as indicated by the negative values of skin friction in Fig. 13. Four of these measurement locations were on the cylinder and one was on the flare. Within the separated region, the largest absolute magnitude measurement was $|C_{fx}| = 0.00043$, which was 29% of the undisturbed upstream boundary-layer value. These measurements within the separated region are of particular importance due to the scarcity of accurate skin-friction data in separated flows.

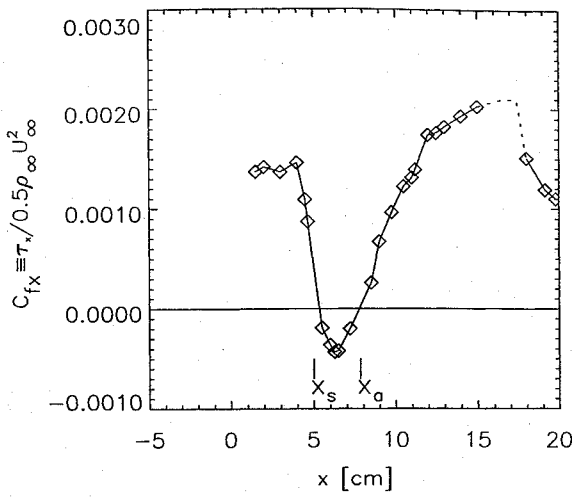

Fig. 13 Streamwise LISF measurements along ϕ = 180 deg.

Interpolation between skin-friction measurements in the vicinity of separation gave a separation location of $x_s = 5.20$ cm. The pressure measurements gave indications of separation at $x_s = 5.25$ cm whereas the oil flow visualization indicated separation was at $x_s = 5.00$ cm. Interpolation of the skin-friction data near attachment indicated the attachment location to be at $x_a = 7.8$ cm which coincided with the attachment location as determined from oil flow visualization. The pressure distribution reached a peak plateau at $x = 9.25$ cm. The maximum skin-friction coefficient of $C_{fx} = 0.00203$ was reached at the most downstream measurement location on the ramp, but the skin friction appeared to still be increasing. This value was 41% larger than the undisturbed level. The peak level along $\phi = 180$ deg was lower than the peak level along $\phi = 0$ probably due to a thicker boundary layer along $\phi = 180$ deg.

Concluding Remarks

An experimental study was conducted on a three-dimensional SW/BLI. The flowfield included a steady shock system and three-dimensional separation with significant crossflow. Surface oil flow visualization was successful in revealing many details of the surface flow topology. A postulated flowfield included two vortices that left the surface near $\phi = 180$ deg and remained embedded in the boundary layer. The pressure documentation was extensive and yielded a contour map of the entire three-dimensional interaction.

The application of the laser interferometric skin friction technique to the flow was significant in many respects. The technique was used to acquire skin-friction data in a complex, compressible flow that included highly swept and separated regions. The LISF instrument yielded a mean skin-friction coefficient of $C_{fx} = 0.00149$ in the upstream, undisturbed boundary layer. The close agreement with two other standards provided assurance of the accuracy of the LISF measurements. The largest source of uncertainty in the LISF results was the measurement of the surface temperature. The skin-friction measurements along $\phi = 0$ downstream of attachment demonstrated an increase of 125% over the upstream value. This increase was greater than along $\phi = 90$ and 180 deg. Documentation of the three-dimensional flow along $\phi = 90$ deg included LISF measurements in the streamwise direction. Transverse skin-friction values were resolved from streamwise LISF measurements and flow-angle data. The resolved data were in close agreement with a limited number of LISF measurements in the transverse direction. Within the separated region along $\phi = 180$ deg, where the flow was opposite to the freestream direction, the maximum absolute value of the skin friction reached a value that was 29% of the undisturbed skin-friction level.

Frequently, only pressure measurements are available from SW/BLI experiments to validate computations. Skin-friction measurements, however, offer a more challenging test for computations since skin friction is a better indication of how the turbulent stresses are modeled. Thus, the present skin-friction measurements considerably enhance the value of this study as a building-block experiment for three-dimensional turbulence modeling and CFD code validation.

References

[1]Wideman, J. K., Brown, J. L., Miles, J. B., and Özcan, O., "Surface Documentation of a Three-Dimensional Supersonic, Shock-Wave/Boundary-Layer Interaction," NASA TM-108824, June 1994.

[2]Brown, J. L., Kussoy, M. I., and Coakley, T. J., "Turbulent Properties of an Axisymmetric Shock-Wave/Boundary-Layer Interaction Flow," International Union of Theoretical and Applied Mechanics Symposium, Paris, France, Sept. 1985; also *Turbulent Shear Layer/Shock-Wave Interactions*, edited by J. Delery, Springer–Verlag, Berlin, 1986, pp. 137–148.

[3]Kussoy, M. I., Brown, J. D., Brown, J. L., Lockman, W. K., and Horstman, C. C., "Fluctuations and Massive Separation in Three-Dimensional Shock-Wave Boundary-Layer Interactions," *Transport Phenomena in Turbulent Flows: Theory, Experiment, and Numerical Simulation; Proceedings of the 2nd International Symposium,* Tokyo, Japan, Oct. 1987, New York, Hemisphere Publishing Corp., 1988, pp. 875–887.

[4]Dunagan, S., Brown, J. L., and Miles, J. B., "A Holographic Interferometry Study of an Axisymmetric Shock-Wave/Boundary-Layer Strong Interaction Flow," *AIAA Journal*, Vol. 25, No. 2, 1987, pp. 294–299.

[5]Brown, J. D., Brown, J. L., Kussoy, M. I., Holt, M., and Horstman, C. C., "Two-Component LDV Investigation of Three-Dimensional Shock/Turbulent Boundary Layer Interactions," *AIAA Journal*, Vol. 26, No. 1, 1988, pp. 52–56.

[6]Olsen, M. E., and Seegmiller, H. L., "Low Aspect Ratio Wing Code Validation Experiment," *AIAA Journal*, Vol. 31, No. 10, 1993, pp. 1744–1752.

[7]Tanner, L. H., and Blows, L. G., "A Study of the Motion of Oil Films on Surfaces in Air Flow, with Application to the Measurement of Skin Friction," *Journal of Physics E: Scientific Instruments*, Vol. 9, No. 3, 1976, pp. 194–202.

[8]Monson, D. J., Driver, D. M., and Szodruch, J., "Application of a Laser Interferometer Skin-Friction Meter in Complex Flows," *Proceedings of the International Congress on Instrumentation in Aeronautics Simulation Facilities*, Sept. 1981, pp. 232–243.

[9]Westphal, R. V., Bachalo, W. D., and Houser, M. H., "Improved Skin Friction Interferometer," NASA TM-88216, March 1986.

[10]Kim, K.-S., and Settles, G. S., "Skin Friction Measurements by Laser Interferometry in Swept Shock Wave/Turbulent Boundary-Layer Interactions," *AIAA Journal*, Vol. 28, No. 1, 1990, pp. 133–139.

[11]Seto, J., and Hornung, H., "Two-Directional Skin Friction Measurement Utilizing a Compact Internally-Mounted Thin-Liquid-Film Skin Friction Meter," AIAA Paper 93-0180, Jan. 1993.

[12]Monson, D. J., Mateer, G. G., and Menter, F. R., "Boundary-Layer Transition and Global Skin Friction Measurement with an Oil-Fringe Imaging Technique," Society of Automotive Engineers, Paper 932550, Sept. 1993.

[13]Bouslog, S., private communication, Lockheed Engineering and Sciences, Houston, TX, 1991.

[14]Berezin, I. S., and Zhidkov, N. P., *Computing Methods*, Pergamon Press, New York, 1965, pp. 442–447.

[15]Peake, D. J., and Tobak, M., "Three-Dimensional Interactions and Vortical Flows with Emphasis on High Speeds," NASA TM-81169, March 1980.

[16]Chapman, G. T., "Topological Classification of Flow Separation on Three-Dimensional Bodies," AIAA Paper 86-0485, Jan. 1986.

[17]Batcho, P., and Sullivan J., "The Three-Dimensional Flowfield in a Supersonic Shock Boundary Layer Corner Interaction," AIAA Paper 88-0307, Jan. 1988.

[18]Cambier, L., and Escande, B., "Calculation of a Three-Dimensional Shock Wave-Turbulent Boundary-Layer Interaction," *AIAA Journal*, Vol. 28, No. 11, Nov. 1990, pp. 1901–1908.

[19]Sun, C.-C., and Childs, M. E., "Flowfield Analysis for Successive Oblique Shock Wave-Turbulent Boundary Layer Interactions," NASA CR-2656, March 1976.

[20]Hopkins, E. J., "Charts for Predicting Turbulent Skin Friction from the Van Driest Method (II)," NASA TN-D-6945, Oct. 1972.